JCI The Journal of Clinical Investigation

Loss of TFF1 is associated with activation of NF-κB–mediated inflammation and gastric neoplasia in mice and humans

Mohammed Soutto, … , Richard M. Peek Jr., Wael El-Rifai

J Clin Invest. 2011;121(5):1753-1767. https://doi.org/10.1172/JCI43922.

Research Article **Oncology**

Trefoil factor 1 (*TFF1*) is a tumor suppressor gene that encodes a peptide belonging to the trefoil factor family of protease-resistant peptides. Although TFF1 expression is frequently lost in gastric carcinomas, the tumorigenic pathways this affects have not been determined. Here we show that *Tff1*-knockout mice exhibit age-dependent carcinogenic histological changes in the pyloric antrum of the gastric mucosa, progressing from gastritis to hyperplasia, low-grade dysplasia, high-grade dysplasia, and ultimately malignant adenocarcinoma. The histology and molecular signatures of gastric lesions in the *Tff1*-knockout mice were consistent with an inflammatory phenotype. In vivo, ex-vivo, and in vitro studies showed that TFF1 expression suppressed TNF-α–mediated NF-κB activation through the TNF receptor 1 (TNFR1)/IκB kinase (IKK) pathway. Consistent with these mouse data, human gastric tissue samples displayed a progressive decrease in TFF1 expression and an increase in NF-κB activation along the multi-step carcinogenesis cascade. Collectively, these results provide evidence that loss of TFF1 leads to activation of IKK complex–regulated NF-κB transcription factors and is an important event in shaping the NF-κB–mediated inflammatory response during the progression to gastric tumorigenesis.

Loss of TFF1 is associated with activation of NF-κB–mediated inflammation and gastric neoplasia in mice and humans

Mohammed Soutto,[1] Abbes Belkhiri,[1] M. Blanca Piazuelo,[2] Barbara G. Schneider,[2] DunFa Peng,[1] Aixiang Jiang,[3] M. Kay Washington,[4] Yasin Kokoye,[5] Sheila E. Crowe,[6] Alexander Zaika,[1,7] Pelayo Correa,[2] Richard M. Peek Jr.,[2] and Wael El-Rifai[1,7]

[1]Department of Surgery, [2]Division of Gastroenterology, [3]Department of Biostatistics, [4]Department of Pathology, and [5]Division of Animal Care, Vanderbilt University Medical Center, Nashville, Tennessee, USA. [6]Division of Gastroenterology and Hepatology, University of Virginia, Charlottesville, Virginia, USA. [7]Department of Cancer Biology, Vanderbilt University Medical Center, Nashville, Tennessee, USA.

Trefoil factor 1 (*TFF1*) is a tumor suppressor gene that encodes a peptide belonging to the trefoil factor family of protease-resistant peptides. Although TFF1 expression is frequently lost in gastric carcinomas, the tumorigenic pathways this affects have not been determined. Here we show that *Tff1*-knockout mice exhibit age-dependent carcinogenic histological changes in the pyloric antrum of the gastric mucosa, progressing from gastritis to hyperplasia, low-grade dysplasia, high-grade dysplasia, and ultimately malignant adenocarcinoma. The histology and molecular signatures of gastric lesions in the *Tff1*-knockout mice were consistent with an inflammatory phenotype. In vivo, ex-vivo, and in vitro studies showed that TFF1 expression suppressed TNF-α–mediated NF-κB activation through the TNF receptor 1 (TNFR1)/IκB kinase (IKK) pathway. Consistent with these mouse data, human gastric tissue samples displayed a progressive decrease in TFF1 expression and an increase in NF-κB activation along the multi-step carcinogenesis cascade. Collectively, these results provide evidence that loss of TFF1 leads to activation of IKK complex–regulated NF-κB transcription factors and is an important event in shaping the NF-κB–mediated inflammatory response during the progression to gastric tumorigenesis.

Introduction

Gastric cancer remains the fourth most common cancer worldwide and the second leading cause of cancer-related deaths. The most common form of gastric cancer is intestinal-type gastric adenocarcinoma, which progresses through a cascade of gastric carcinogenesis from normal mucosa to chronic superficial gastritis, atrophic gastritis, intestinal metaplasia with low- and high-grade dysplasia (LGD and HGD, respectively), and invasive gastric adenocarcinoma (1). Infection with *H. pylori*, a class 1 carcinogen according to WHO classification, is the main risk factor. Nonetheless, other risk factors such as a high-salt diet, lack of fruit and vegetable intake, and genetics of the host and the bacterium interact to dictate the outcome in a population. This complexity continues to challenge our understanding of the biology of this devastating cancer.

The trefoil peptides (trefoil factor 1 [TFF1], TFF2, and TFF3) are a group of highly conserved small proteins that are localized within mucous granules in mucus-secreting cells and are expressed and secreted by epithelial cells that line mucous membranes (2). TFF1 is expressed predominantly by the gastric epithelia, in the upper portion of the glandular pits, and is ectopically expressed in some adenocarcinomas such as breast cancer (2–4). In the breast, TFF1 expression is highly expressed in estrogen receptor–positive tumors and inversely associated with histological grade (4). In the stomach, TFF1 is secreted to become a component of the protective mucus layer. TFF1 is synthesized and secreted by the mucus-secreting pit cells of the corpus and antropyloric regions of the stomach (2, 5). TFF1 expression is strongly induced after mucosal injury (6) and is involved in stomach ontogenesis and maintenance of the integrity of the mucosa (2, 3). Molecular studies have shown frequent loss of TFF1 expression in more than two-thirds of gastric carcinomas resulting from a mutation-independent mechanism (7–9). The silencing of the *TFF1* gene in gastric carcinomas is due to loss of heterozygosity (LOH) and methylation of the *TFF1* promoter region (7, 10–13), but mutations are seen only in approximately 5% of gastric carcinomas (7, 14). Silencing of *Tff1* could also be triggered by chromatin remodeling associated with histone modifications, such as H3K9 methylation and H3 deacetylation at the *Tff1* promoter, as seen in *N*-methyl-*N*-nitrosourea–induced gastric carcinogenesis mouse model (13). In addition, transcriptional repression of TFF1 in gastric epithelial cells by CCAAT/enhancer binding protein-β (15) and cofactor of BRCA1 has been demonstrated (9). A number of studies have shown that *TFF1* is a candidate tumor suppressor gene that inhibits cell growth (16). The *Tff1*-knockout mouse model provided the first evidence supporting a tumor suppressor role of Tff1 in gastric tumorigenesis, demonstrating that it is essential for normal differentiation of the antral and pyloric gastric mucosa (17). The spectrum of histological lesions and the mechanisms and molecular pathways that are mediated by the loss of TFF1 in gastric tumorigenesis are still not fully elucidated.

NF-κB transcription factors are important in integrating multiple stress stimuli and regulating immune responses (18, 19). A large body of evidence suggests that NF-κB is one of the few key regulatory signaling molecules, the aberrant activation of which is invariably associated with inflammation and cancer (20). The NF-κB transcription factors, regulated via the IκB kinase (IKK) complex, play a critical role in coupling inflammation and cancer

Conflict of interest: The authors have declared that no conflict of interest exists.
Citation for this article: *J Clin Invest.* 2011;121(5):1753–1767. doi:10.1172/JCI43922.

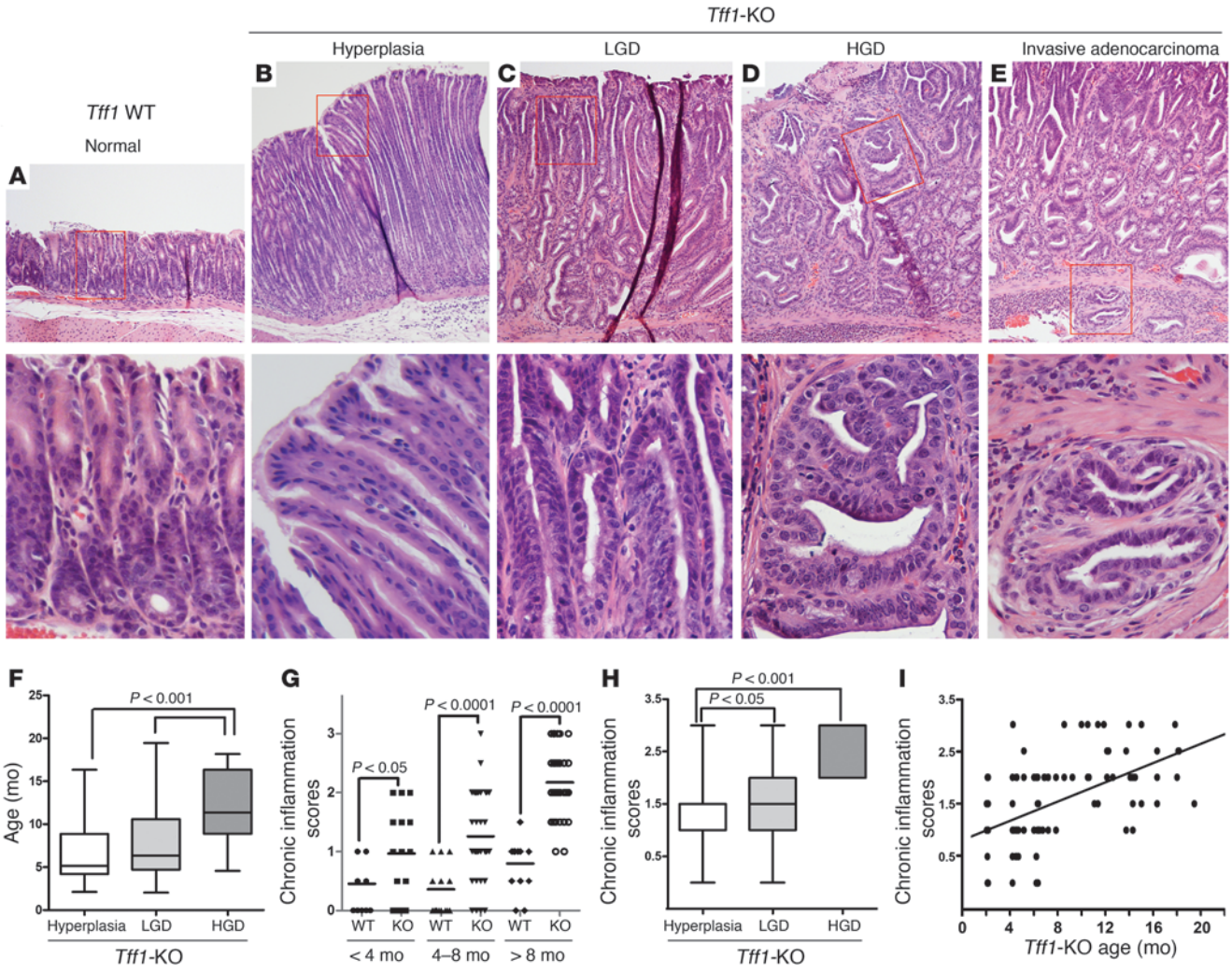

Figure 1

Loss of the *Tff1* gene promotes susceptibility to inflammation and gastric tumorigenesis. (**A**–**E**) H&E staining of representative histological features of gastric mucosa from wild-type (normal; **A**) and *Tff1*-knockout mice showing progressively more severe lesions: hyperplasia (**B**), LGD (**C**), HGD (**D**), and invasive adenocarcinoma (**E**). Original magnification, ×10 (top), ×40 (bottom). (**F**) Box plots representing the progression of lesions as a function of age in *Tff1*-knockout mice. (**G**–**I**) Chronic inflammation scores. (**G**) Comparison of matched ages between wild-type and *Tff1*-knockout mice; each data point represents a single mouse, and the horizontal bars denote the mean value. (**H**) Box plot showing increase of inflammation from hyperplasia to LGD to HGD. (**I**) Pearson's correlation test between chronic inflammation and age in *Tff1*-knockout mice. Box-and-whisker plots used in **F** and **H** depict the smallest value, lower quartile, mean, upper quartile, and largest value.

(21). The specific activation of the IKK/NF-κB pathway promotes formation of inflammation-associated tumors and suppresses apoptosis in advanced tumors (22). Activated nuclear NF-κB is a crucial mediator of inflammation-induced tumor growth and progression, as well as an important modulator of tumor surveillance and rejection (23). NF-κB activation promotes cell survival through induction of pro-survival target genes and genes encoding antioxidant proteins in normal and cancerous cells (24). However, mechanisms and pathways responsible for NF-κB activation in gastric carcinomas remain unknown. Using the *Tff1*-knockout mouse model together with several in vivo, ex-vivo, and in vitro experiments, we provide what we believe is the first molecular evidence that TFF1 plays an important role in regulating the NF-κB–mediated inflammatory response in the multistep gastric tumorigenesis cascade.

Results

Histological evidence of multi-step progression toward gastric cancer in the Tff1-knockout mice. Gross pathology of the stomach revealed nodular mucosa in the antropyloric of the stomach in *Tff1*-knockout mice at the age of 6 months and up (Supplemental Figure 1A; supplemental material available online with this article; doi:10.1172/JCI43922DS1). Histological analysis using H&E staining indicated a sequence of morphological changes that included hyperplasia, LGD, HGD, and finally invasive neoplasia that were observed in pyloric antra of *Tff1*-knockout mice and not in *Tff1* wild-type mice (Figure 1, A–E). The progression of changes was age dependent as shown in Figure 1F. At the age of 2 months, the *Tff1*-knockout mice displayed marked glandular hyperplasia with elongated pits that occupied most of the thickness of the mucosa (Figure 1B). The average age for the development of LGD was around

6 months and was characterized by branching and elongation of crypts and crowded nuclei that maintain polarity with respect to the basement membrane (Figure 1C). The HGD appeared to be frequent at the age of 8 months and up. HGD was characterized by glandular and nuclear contour irregularity and by enlarged and hyperchromatic nuclei with loss of polarity with respect to the basement membrane. Some glands showed cribriform structures with marked reduction of the interglandular stroma (Figure 1D). In 5 mice aged 8 months or older, the neoplastic antropyloric tissues of the *Tff1*-knockout mice expanded progressively into the submucosa through gaps in the muscularis mucosa and formed invasive adenocarcinomas (Figure 1E). There were no ulcerative lesions at any time point. To investigate the characteristics of the antropyloric lesions, we immunostained gastric tissues for the proliferation-associated marker Ki-67. In the *Tff1* wild-type stomach tissue, Ki-67 staining was seen in the proliferative zone at the basal third of the glands or crypts (Supplemental Figure 1B). The *Tff1*-knockout stomach lesions at the hyperplasia stage and the more advanced cyst-like structures in dysplasia were composed mostly of highly proliferating cells that extended to the surface of the mucosa (Supplemental Figure 1B).

Spontaneous and progressive inflammation in the gastric mucosa of the Tff1-knockout mice. The H&E-stained sections showed inflammatory cell infiltration in all the lesions studied. To assess the relationship between inflammatory cell infiltration and tumor progression, we first compared chronic and acute inflammation in gastric tissue samples from *Tff1* wild-type ($n = 44$) and *Tff1*-knockout mice ($n = 126$). We found that both inflammation scores were higher in *Tff1*-knockout gastric tissues than in those of *Tff1* wild-type mice ($P < 0.001$) (Supplemental Figures 1, C and D). Next, we determined chronic inflammation scores in matching age in both groups. We found that the inflammation scores in *Tff1*-knockout mice increased significantly ($P < 0.05$) with age. However, there was no significant difference between different age groups in *Tff1* wild-type mice (Figure 1G). Also, we compared inflammation in *Tff1*-knockout gastric tissues in males versus females. There was no significant difference between genders in either type of inflammation (Supplemental Figures 1, E and F). Further, we evaluated inflammation scores at different stages of tumor progression. As shown in Figure 1H and Supplemental Figure 1G, inflammation increased with progression of the lesions from hyperplasia to LGD to HGD; the HGD also include adenocarcinoma. To extend our histopathological analysis, we evaluated chronic inflammation with respect to age. Our data demonstrated a positive correlation between inflammation and age (coefficient $r = 0.6$; $P < 0.001$) (Figure 1I). Thus, the aforementioned results suggest that inflammation and age both play an important role in tumor progression in *Tff1*-knockout mice.

In order to exclude the possible effect of pathogens on the inflammation scores, 2-week-old weaned *Tff1*-knockout mice and *Tff1* wild-type mice were treated with a combination of the antibiotic ciprofloxacin (0.34 mg/ml) and the antibiotic and antiprotozoal metronidazole (0.68 mg/ml) in drinking water until the age of 12 weeks. This treatment was then discontinued, and mice received autoclaved water and rodent chow for 12 weeks. This treatment did not disrupt the increase of inflammation scores in *Tff1*-knockout mice as compared with *Tff1* wild-type mice (Supplemental Figure 1H). We next checked the histology in different tissues in the gastrointestinal tract (stomach, esophagus, colon), and other organs such as liver spleen and thymus from the same *Tff1*-knockout mice. We confirmed that the inflammation and lesions were specifically located in the pyloro-antral region of the stomach (Supplemental Figure 2A) but not in other examined tissues (Supplemental Figure 2, B–F).

Gene expression profiling identifies NF-κB activation as a mediator of disease progression. We next sought to identify genes whose expression signature was associated with loss of Tff1 by profiling mRNA extracted from laser capture microdissected antral epithelial cells of *Tff1*-knockout mice and from age-matched *Tff1* wild-type mice. Using microarrays, we identified 636 genes that were upregulated or downregulated by more than 2.8-fold with a significance level of $P \leq 0.05$. We then generated a heat map by performing a hierarchical clustering analysis of these genes. We found a distinct molecular signature that distinguishes the *Tff1*-knockout gastric tissues from *Tff1* wild-type tissues (Figure 2A). To understand the relationships between the 636 genes identified in this study and the physiologic function, we utilized the Ingenuity Pathway Analysis software (Ingenuity Systems, Inc.). This analysis revealed NF-κB to be a network hub that is activated in *Tff1*-knockout mice (Figure 2B). Taken together, these findings suggest a possible role for the NF-κB pathway in initiating gastric cancer in the *Tff1*-knockout mouse model. Interestingly, a close examination revealed 76 genes that are related to inflammation (Supplemental Table 1). All pro-inflammatory genes were found to be upregulated, and only few anti-inflammatory genes were downregulated. In order to validate the results of our expression microarrays, we performed quantitative real-time RT-PCR (qRT-PCR) analysis of 8 differentially expressed pro-inflammatory genes *Tnfa*, *Il1b*, *Il1a*, *Cxcl1*, *Cxcl2*, *Cxcl5*, *Il4r*, and *Vtcn1*, and 1 anti-inflammatory gene (*Apoa1*). The results of qRT-PCR of these genes were analyzed according to the status of stomach lesions in the *Tff1*-knockout gastric tissues (LGD/HGD) compared with histologically normal gastric mucosa from the *Tff1* wild-type mice. Interestingly, the qRT-PCR results showed a significant progressive increase in the expression levels of the 8 pro-inflammatory genes (Figure 3, A–H) and a decrease in the anti-inflammatory gene *Apoa1* (Figure 3I). We further analyzed qRT-PCR results according to the age of the mice; the *Tff1* wild-type and *Tff1*-knockout mice were separated into 2 groups: the first group was 2–6 months old, and the second was at least 8 months old. In wild-type mice, there was no significant difference in the expression of the inflammatory genes in the 2 age groups (data not shown). Consequently, we combined all wild-type control mice to compare them with the 2 age groups of *Tff1*-knockout mice. This analysis showed a significant upregulation of the 8 identified pro-inflammatory genes in the *Tff1*-knockout mice compared with *Tff1* wild-type mice. Indeed, this upregulation was observed in older animals when comparing the 2 age groups of *Tff1*-knockout mice (Supplemental Figure 3, A–H). Concordant with these findings, expression of the *Apoa1* gene showed a significant downregulation with age progression when compared with *Tff1* wild-type (Supplemental Figure 3I).

To investigate whether the tumor progression in *Tff1*-knockout mice was an inflammation-associated event, we used celecoxib, a selective Cox-2 inhibitor and nonsteroidal anti-inflammatory drug (NSAID). *Tff1*-knockout mice were injected i.p with vehicle (5 μl/g body weight) as a control or celecoxib (10 μg/g; 5 μl vehicle/g). Treatment was started after weaning at the age of 3 weeks and lasted until 12 weeks of age. Histopathological assessment revealed gastric dysplasia in 9 of 10 (90%) mice in the control group injected with vehicle. However, only 4 of 10 mice (40%) in the celecoxib-injected group

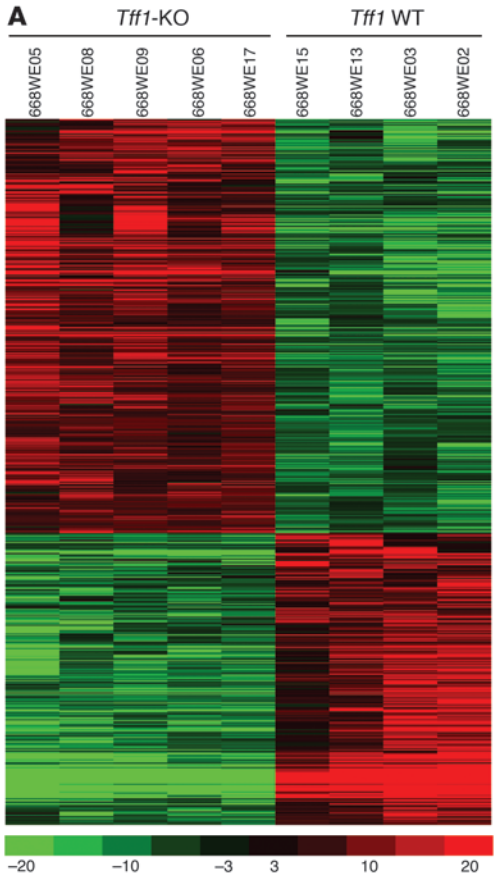

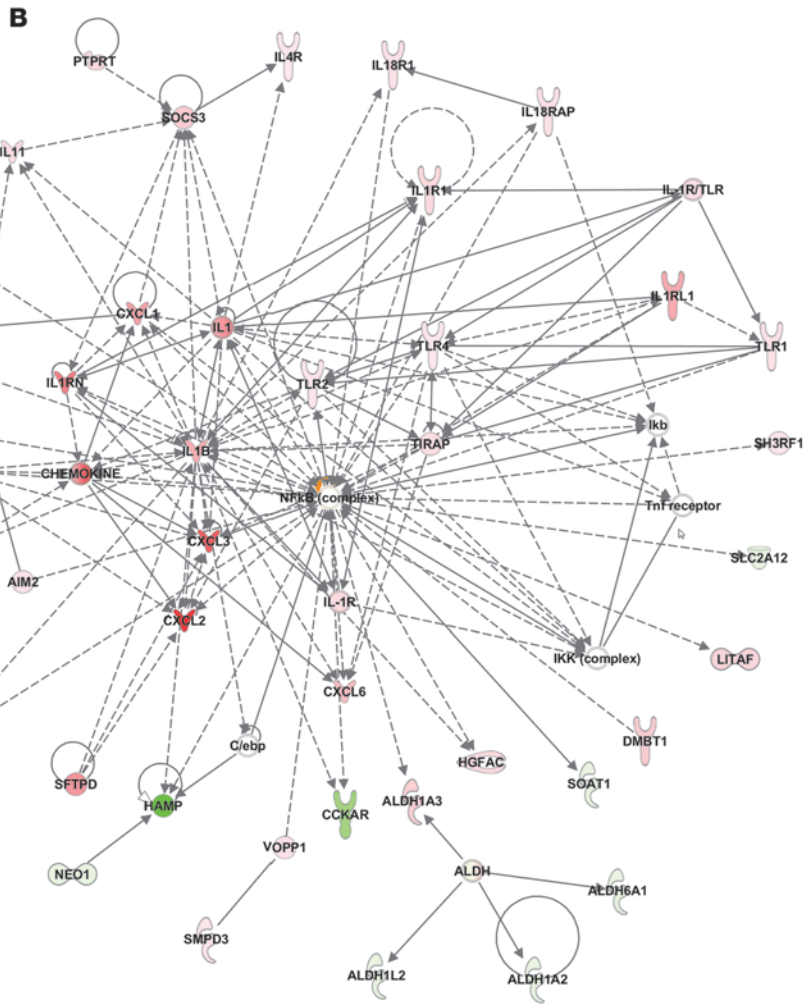

Figure 2

Molecular signatures in the *Tff1*-knockout gastric tissues. (**A**) Heat map showing the hierarchical clustering of 636 genes that had significant changes (≥2.8-fold; $P \leq 0.05$). Red and green indicate relative upregulation or downregulation of genes, respectively. (**B**) Network analysis predicted by Ingenuity Pathway Analysis in *Tff1*-knockout mice. As shown, the analysis of the 636 differentially expressed genes indicated a central role for the NF-κB network in the *Tff1*-knockout gastric tissues as compared with wild-type tissues. Several inflammatory genes with differentially regulated mRNA expression levels are shown.

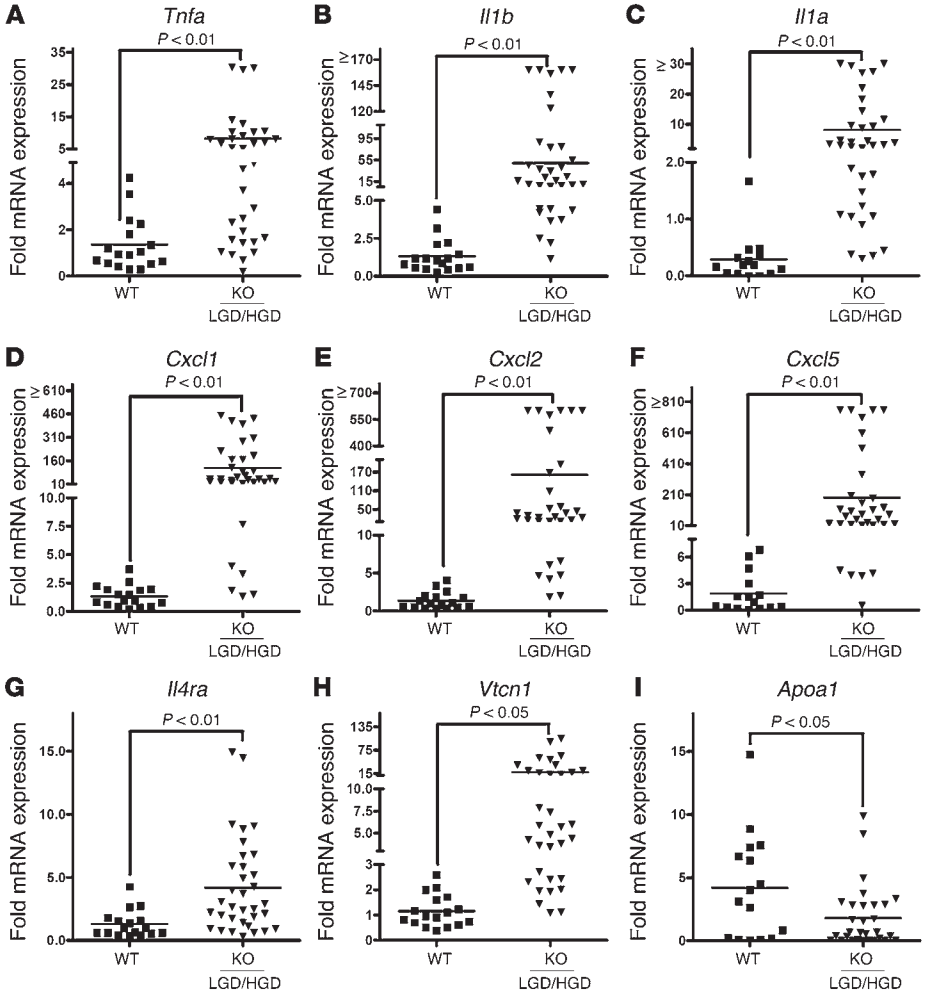

Figure 3
Expression of inflammation-related genes. (**A**–**I**) Validation of microarray results by qRT-PCR analysis of 9 inflammation-related genes. (**A**–**H**). The pro-inflammatory genes (*Tnfa*, *Il1b*, *Il1a*, *Cxcl1*, *Cxcl2*, *Cxcl5*, *Il4ra*, and *Vtcn1*) showed upregulation in LGD/HGD gastric tissues from the *Tff1*-knockout mice as compared with normal gastric tissues from the wild-type mice. (**I**) The anti-inflammatory gene *Apoa1* showed downregulation in LGD/HGD gastric tissues from the *Tff1*-knockout mice as compared with normal gastric tissues from the wild-type mice. Horizontal bars indicate the mean values. $P < 0.05$ was considered statistically significant.

developed gastric dysplasia (Supplemental Figure 4A) restricted to the antropyloric region. Also, we examined the expression of two pro-inflammatory genes, *Cxcl1* and *Cxcl5*, using qRT-PCR. Both genes showed a statistically significant decrease of expression in the celecoxib-treated group compared with the vehicle group (Supplemental Figure 4, B and C), suggesting that the tumorigenesis in *Tff1*-knockout mice is associated with inflammation.

TFF1 regulates nuclear localization of NF-κB in in vivo and in vitro models. The NF-κB pathway is activated in several inflammation-linked cancers (23, 25). The excessive activation of NF-κB leads to overproduction of pro-inflammatory cytokines and chemokines and chronic inflammation (26). Because of the inflammatory phenotype and molecular signature obtained in the *Tff1*-knockout gastric tissues, we next asked whether loss of Tff1 induced nuclear localization and activation of NF-κB. To address this hypothesis, we isolated primary gastric epithelial cells from the pyloric antral region of *Tff1* wild-type and *Tff1*-knockout mice stomachs. Immunofluorescence staining on short-term–cultured cells demonstrated a significant increase (approximately 3-fold) in nuclear p65 staining in *Tff1*-knockout epithelial cells as compared with *Tff1* wild-type (P <0.001) (Figure 4, A and B).

Next, we reconstituted the expression of TFF1 in the AGS human gastric adenocarcinoma cell line as an in vitro cell model to validate our findings and establish the mechanism of NF-κB activation. Two separate AGS cell clones that stably express *TFF1*, as confirmed by qRT-PCR, were included in this study (Supplemental Figure 5A). The AGS-TFF1 clones demonstrated diminished nuclear p65 staining as compared with empty vector AGS-pcDNA (control) (Figure 4C). Quantification of more than 200 cells from different fields showed a significantly higher percentage of nuclear NF-κB–positive cells in AGS-pcDNA control (85%) than AGS-TFF1 clone 1 (25%) and clone 2 (35%) ($P < 0.01$), as shown in Figure 4D. Taken together, the *Tff1*-knockout mouse model and the in vitro and ex-vivo cell models suggest that TFF1 is a negative regulator of NF-κB signaling.

TFF1 suppresses TNF-α–mediated NF-κB transcription activity. To fully define the role of TFF1 in regulating the activity of the NF-κB signaling pathway, we examined the effect of TFF1 on the transcriptional activity of NF-κB using the pNF-κB–Luc reporter, which contains multiple copies of the NF-κB consensus sequence. The pNF-κB–Luc reporter is designed to measure the binding of NF-κB to κ enhancer elements, providing a direct measurement of activation of the NF-κB pathway (27). The empty vector AGS-pcDNA and the AGS-TFF1 clones were transfected with pNF-κB–Luc and treated with TNF-α (50 ng/ml) for 24 hours. The AGS-TFF1 clones showed a diminished activation of the pNF-κB–Luc following TNF-α stimulation, as compared with AGS-pcDNA control (Figure 5A). In addition, we confirmed the suppressive effect of TFF1 on NF-κB

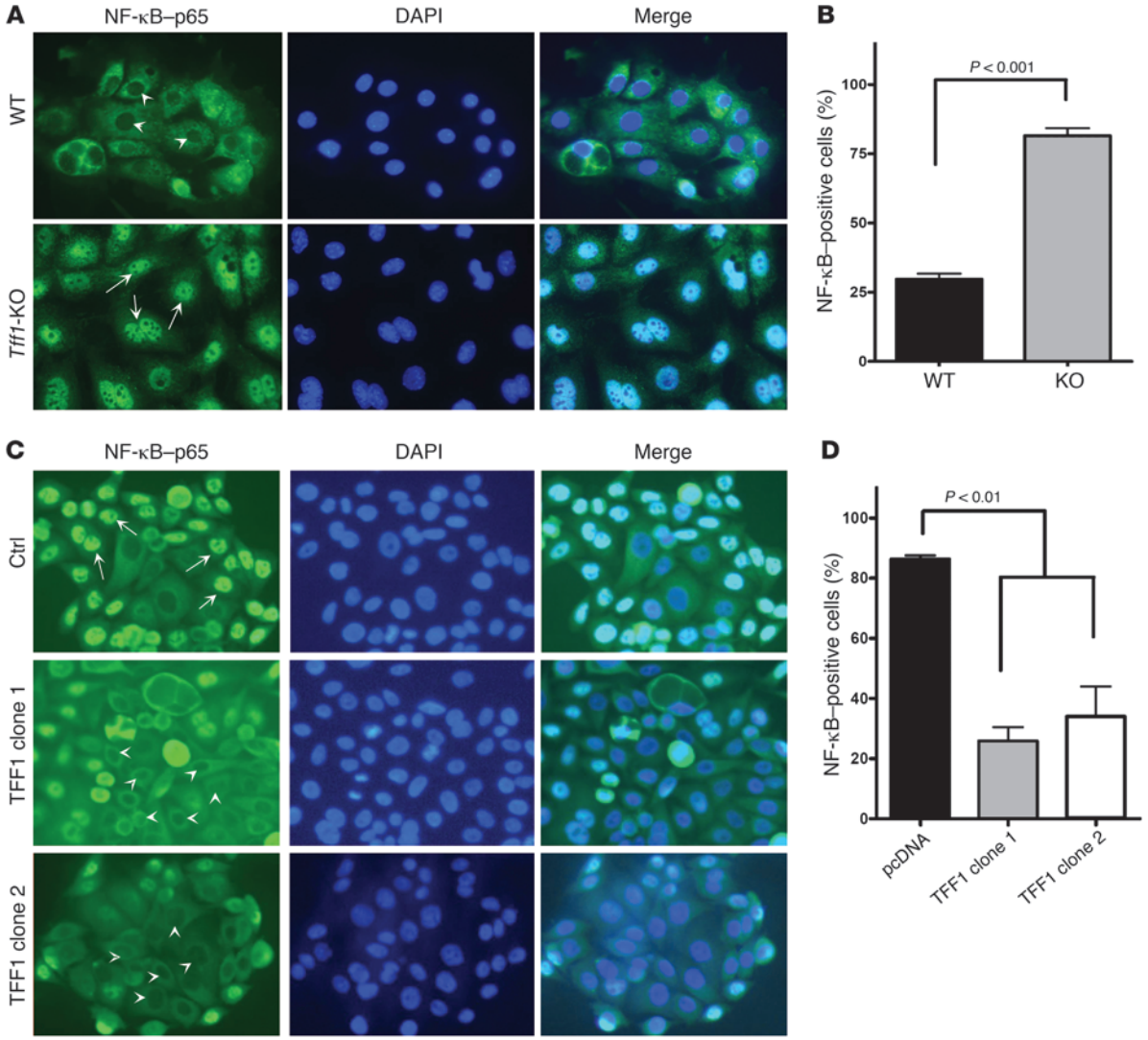

Figure 4

TFF1 expression negatively regulates NF-κB activation. (**A**) Ex vivo immunofluorescence assay in primary gastric epithelial cells isolated from the antrum of *Tff1*-knockout and wild-type mice at 2 months of age, demonstrating the nuclear localization of NF-κB–p65 (green) immunostaining (arrows) in *Tff1*-knockout but not in *Tff1* wild-type cells (arrowheads). DAPI (blue) was used a nuclear counterstain. Original magnification, ×40. (**B**) Graph showing the quantification of nuclear NF-κB–p65 positive staining in at least 200 counted cells presented as percentage ± SEM. (**C**) In vitro immunofluorescence assay showing nuclear localization of NF-κB–p65 (arrows) in AGS-pcDNA or absence of nuclear staining (arrowheads) in AGS-TFF1 (clones 1 and 2) after 24 hours of cell culture. DAPI (blue) was used as a nuclear counterstain. Original magnification, ×40. (**D**) Graph showing the quantification of nuclear NF-κB–p65–positive staining in at least 200 counted cells presented as percentage ± SEM.

activity by treating the parental AGS cells with recombinant TFF1 protein (400 ng/ml) and/or TNF-α for 24 hours. The NF-κB activity in the parental AGS cells treated with both TFF1 and TNF-α was reduced by 75% compared with the parental AGS cells treated with TNF-α alone (Figure 5B). Furthermore, we performed another assay to confirm the inhibitory effect of TFF1 on NF-κB activity by treating AGS parental cells with conditioned media from the AGS-TFF1 or empty vector AGS-pcDNA clones that were simultaneously stimulated with TNF-α (50 ng/ml) for 24 hours. Luciferase activity in AGS parental cells treated with conditioned media from both the AGS-TFF1 clone and TNF-α was reduced by 45% compared with parental AGS cells treated with conditioned media from both AGS-pcDNA and TNF-α (Figure 5C). Immunofluorescence using NF-κB–p65 antibody, with quantification of 200 cells from different fields, also showed significantly less NF-κB nuclear staining in both AGS-TFF1 clones (25% in clone 1 and 35% in clone 2) after stimulation with TNF-α compared with empty vector AGS-pcDNA (85%) (Figure 5, D and E). Collectively, these data from ex vivo and in vitro studies suggest that TFF1 regulates the NF-κB transcription activity in gastric epithelial cells.

TFF1 inhibits TNF-α–mediated IκB phosphorylation. Phosphorylation of IκB by the IKK complex is a key step for the nuclear localization of NF-κB subunits (28). Because IKK activation by phosphorylation is essential for TNF-α–induced NF-κB activation, we measured IKK phosphorylation following TNF-α treatment in AGS-TFF1 and AGS-pcDNA clones. As shown in Figure 6, A and B,

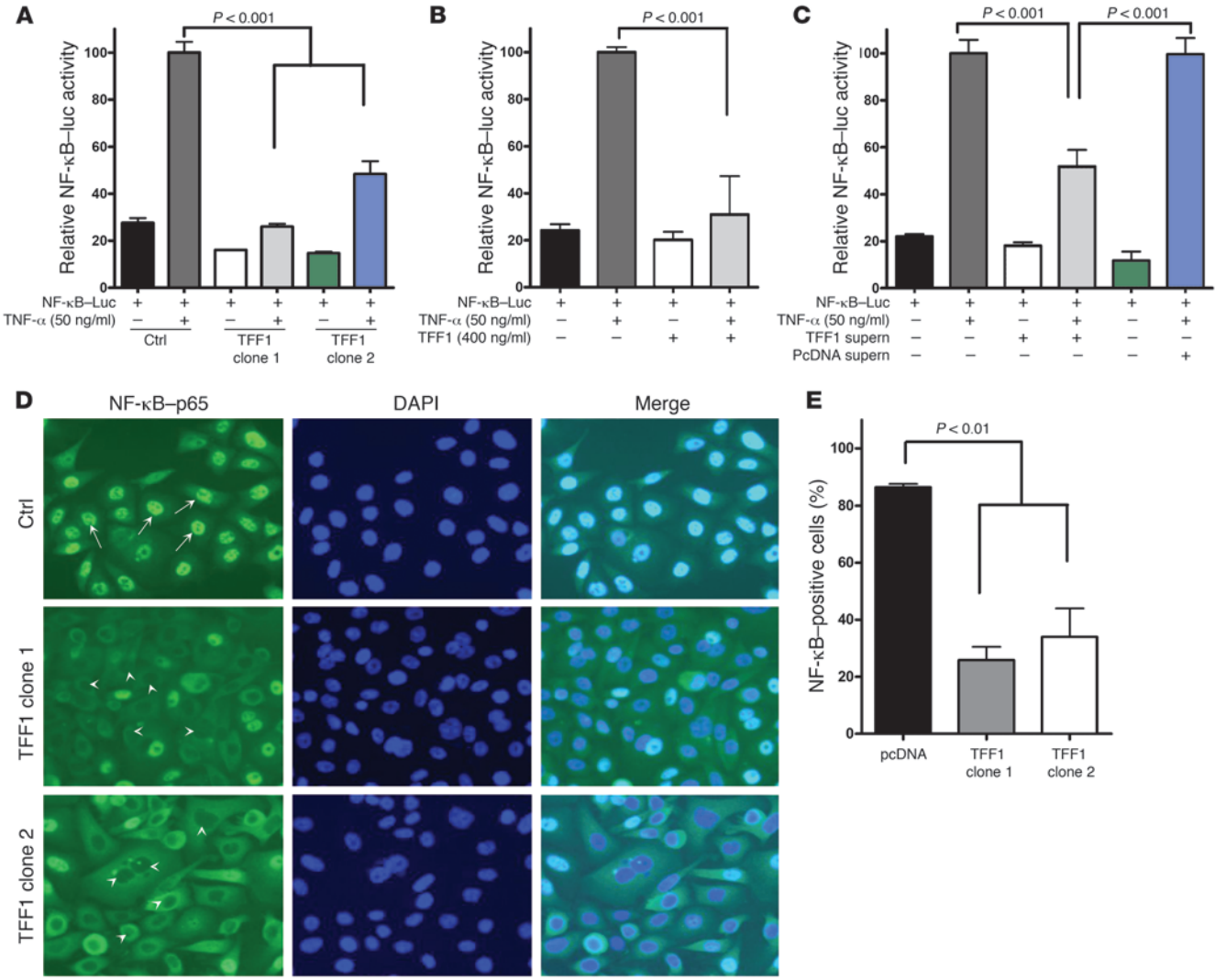

Figure 5

TFF1 overexpression alters TNF-α–mediated NF-κB–p65 activation. (**A**–**C**) The luciferase reporter assay using a pNF-κB–Luc reporter plasmid. (**A**) AGS-TFF1 cells (clones 1 and 2) were co-transfected with pNF-κB–firefly luciferase reporter and Renilla luciferase and stimulated with TNF-α (50 ng/ml). The AGS-pcDNA was used as a positive control. (**B**) AGS wild-type cells were transfected with pNF-κB–firefly luciferase and Renilla luciferase and stimulated with either TNF-α (50 ng/ml) or TFF1 (400 ng/ml) or both. (**C**) The effect of conditioned media from AGS-TFF1 (clone 1) on TNF-α mediated NF-κB promoter activity in AGS wild-type cells transfected with pNF-κB–firefly luciferase and Renilla luciferase. The AGS-pcDNA–conditioned media was used as a control. Data are presented as mean ± SEM of at least 3 experiments, with each condition performed in triplicate. (**D**) In vitro immunofluorescence assay of AGS-pcDNA and AGS-TFF1 clones 1 and 2, stimulated with TNF-α (50 ng/ml) for 24 hours, indicating nuclear localization of NF-κB–p65 (green fluorescence, arrows) in AGS-pcDNA and absence of nuclear NF-κB–p65 staining (arrowheads) in AGS-TFF1 (clones 1 and 2). DAPI (blue) was used as a nuclear counterstain. Original magnification, ×40. (**E**) Graph shows the quantification of nuclear NF-κB–p65–positive staining in at least 200 counted cells, with results presented as percentage ± SEM.

phosphorylation of IKKα/β (Ser176/180) was quickly activated in AGS-pcDNA cells in response to TNF-α treatment. In contrast, IKKα/β phosphorylation was not significantly activated in AGS-TFF1 clones (Figure 6C).

IKK is responsible for IκB phosphorylation and ubiquitination, which is a crucial step for TNF-α–induced IκB degradation and NF-κB–p65 activation (21, 29). We next examined IκB phosphorylation following TNF-α treatment. Phosphorylation of IκB (Ser32) at 5 minutes following TNF-α treatment was higher in AGS-pcDNA as compared with AGS-TFF1 clones (Figure 6, A and B). As expected, this phosphorylation was followed by a rapid disappearance of IκB protein in AGS-pcDNA cells at 10 minutes, indicative of the rapid degradation of IκB as a result of its phosphorylation (Figure 6, A and B).

The subcellular localization of NF-κB–p65 following TNF-α stimulation in AGS-TFF1 and AGS-pcDNA cells was determined by immunofluorescence at 0, 10, and 30 minutes. At time 0, we have seen a basal level of nuclear NF-κB staining in AGS-pcDNA that was further reduced in AGS-TFF1 (Figure 6E), which was confirmed by Western blot analysis of IKKα/β phosphorylation relative to the total IKKβ (Supplemental Figure 5B). However, after 10 minutes, there was more significant reduction in the

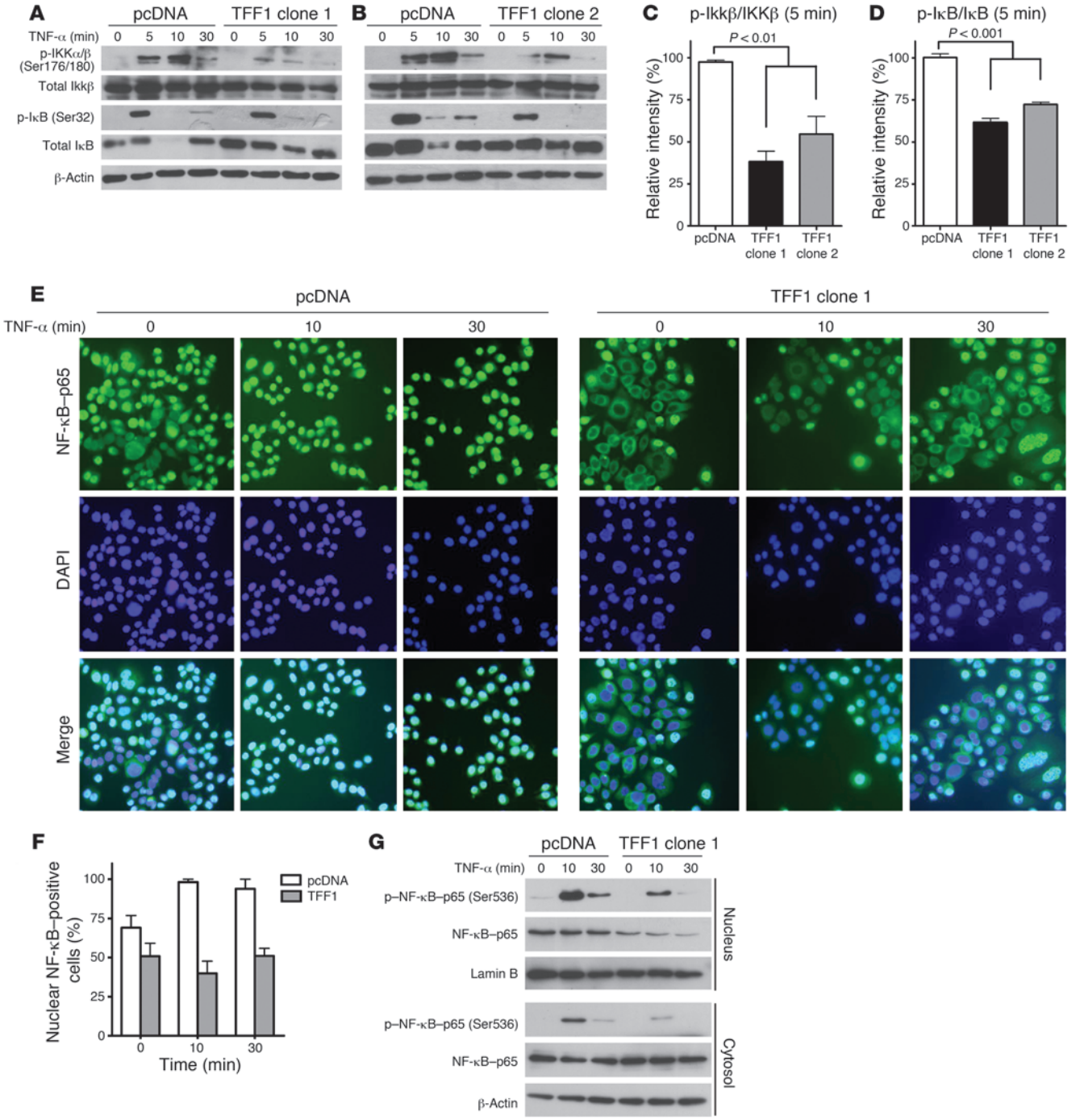

Figure 6

TFF1 negatively regulates TNF-α–induced NF-κB signaling pathway. (**A** and **B**) AGS-pcDNA and AGS-TFF1 clones 1 and 2 were treated with TNF-α (50 ng/ml) for the indicated time points or left untreated as a control. The same amount of proteins from an extract of each cell line was applied to SDS-PAGE for immunoblotting with p-IKKα/β (Ser176/180), total IKKβ, or p-IκB (Ser32) antibodies. Total IKKβ and β-actin were used as loading controls. (**C** and **D**) The relative intensity ratio of p-IKK β/total IKKβ and p-IκB/total IκB at 5 minutes after stimulation with TNF-α are presented as graphs produced from analysis by ImageJ software. The results are expressed as mean ± SEM of at least 3 independent experiments. (**E**) In vitro immunofluorescence assay of AGS-pcDNA and AGS-TFF1 clone 1. Cells were cultured and stimulated with TNF-α (50 ng/ml) for the indicated times. Nuclear localization of NF-κB–p65 is shown in green. DAPI (blue) was used as a nuclear counterstain. Original magnification, ×40. (**F**) Graph shows the quantification of nuclear NF-κB–p65–positive staining in at least 200 counted cells presented as a percentage. Data represent mean ± SEM. (**G**) Protein expression levels of total and p–NF-κB–p65 (Ser536) in the nuclear and cytosolic fractions in AGS-TFF1 clone 1 normalized to Lamin B and β-actin, respectively. The Western blot results represent 1 of 3 independent experiments.

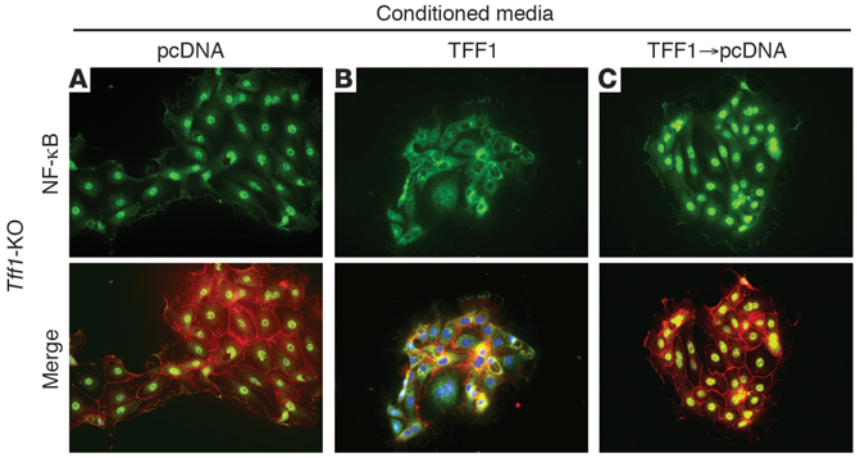

Figure 7
TFF1 negatively regulates NF-κB activity in primary epithelial cells. Ex vivo immunofluorescence assay was performed on primary gastric epithelial cells isolated from the antrum of *Tff1*-knockout mouse. (**A**) Nuclear immunostaining of NF-κB–p65 (green fluorescence) was detected in cells that were treated with conditioned media from AGS-pcDNA cell line for 48 hours. (**B**) Primary gastric epithelial cells treated with conditioned media from AGS-TFF1 cell line for 48 hours displayed loss of nuclear immunostaining of NF-κB–p65. (**C**) On the other hand, gastric epithelial cells treated with conditioned medium from the AGF-TFF1 cell line for 24 hours, followed by replacement of this medium with conditioned medium from AGS-pcDNA cell line for another 24 hours restored the nuclear localization of NF-κB–p65. ZO1 (red) immunostaining was used as an epithelial cell marker, and DAPI (blue) was used as a nuclear counterstain. The results represent 1 of 3 independent experiments. Original magnification, ×40.

percentage of cells with nuclear NF-κB in AGS-TFF1 clones than AGS-pcDNA control (Figure 6, E and F). Results from a Western blot analysis for nuclear and cytosolic protein fractions were consistent with the above findings (Figure 6G). The nuclear protein extracts showed a higher TNF-α–induced phosphorylation of NF-κB–p65 (Ser536) at 10 minutes in AGS-pcDNA cells as compared with the AGS-TFF1 cells. In addition, p–NF-κB–p65 (Ser536) was observed mostly in the nuclear fraction of AGS-pcDNA cells. Whole cytosolic fraction of the AGS-TFF1 cells had a higher level of total NF-κB–p65 than the nuclear fraction. The above experiments confirm that TFF1 abrogates TNF-α–mediated phosphorylation and nuclear localization of NF-κB–p65 in a mechanism that involves IKK/IκB partners.

Activation of NF-κB in primary epithelial cells is driven by loss of Tff1. We examined the *Tff1* mRNA expression in antropyloric region of the stomach, thymus, spleen, and bone marrow in *Tff1* wild-type mice. While the expression level of *Tff1* was high in the stomach, it was low to undetectable in the other organs, indicating that *Tff1* expression is gastric specific (Supplemental Figure 6), thereby suggesting that the inflammatory phenotype in the *Tff1*-knockout mice is possibly independent of immune cells. To confirm the possibly cell-autonomous effect of TFF1 and whether the observed interplay between TFF1 and NF-κB activation may be directly due to the loss of TFF1, we treated primary gastric epithelial cells from *Tff1*-knockout mice with conditioned media from AGS-pcDNA or AGS-TFF1 clones. The results from immunofluorescence experiment indicated that treatment with AGS-pcDNA–conditioned media led to NF-κB–p65 nuclear staining (Figure 7A). In contrast, treatment with AGS-TFF1–conditioned media resulted in loss of NF-κB–p65 nuclear staining (Figure 7B). In addition, in a rescue experiment, the cells that were cultured in AGS-TFF1–conditioned media were washed and then treated with AGS-pcDNA–conditioned media. The immunofluorescence results showed reconstitution of NF-κB–p65 nuclear staining in these cells (Figure 7C).

TFF1 suppresses the expression of pro-inflammatory and pro-survival NF-κB target genes in vitro. The aforementioned NF-κB–Luc reporter, immunofluorescence, and Western blot analyses together all support enhanced transcriptional activation and nuclear localization of NF-κB in AGS-pcDNA cells as compared with AGS-TFF1 cells. Using qRT-PCR, we examined the expression of known NF-κB targets in AGS-TFF1 clones relative to AGS-pcDNA. The results showed a significant decrease in expression levels of pro-inflammatory (*CXCL5*, *TIRAP*, and *IL4RA*) (Figure 8, A–C) and anti-apoptotic genes (*BIRC3* and *SMAC*) (Figure 8, D and E) following 8 hours of TNF-α stimulation in AGS-TFF1 cells compared with AGS-pcDNA cells. These results indicate that TFF1 suppresses NF-κB target genes, further confirming that loss of TFF1 activates NF-κB, which may represent a mechanism by which inflammation promotes gastric cancer.

Because the activation of NF-κB is induced when TNF-α binds to its receptors, TNFR1 and TNFR2, first we asked which of these receptors is important in our gastric cancer cell model. qRT-PCR data revealed that *TNFR1* mRNA was highly expressed in AGS-TFF1 and AGS-pcDNA clones. However, the expression of *TNFR2* was undetectable compared with *TNFR1* when normalized to the housekeeping gene *HPRT* (Supplemental Figure 7A). We next tested the hypothesis that TFF1 may interfere with the recruitment and binding of TRAF2 to TNFR1. Consistent with previous reports (30), TNF-α treatment induced TRAF2 recruitment to the TNFR1 complex in AGS-pcDNA cells (Figure 8F). In contrast, this recruitment was abolished in AGS-TFF1–expressing cells, where TRAF2 was not detected in the TNFR1 protein immunoprecipitate (Figure 8F). In addition, we compared the expression of *Tnfr1* mRNA in the antropyloric region of the stomach in *Tff1*-knockout and *Tff1* wild-type mice, and in AGS-pcDNA and AGS-TFF1 clones. The *TNFR1* mRNA was equally expressed irrespective of *TFF1* expression (Supplemental Figures 7, A and B).

Downregulation of TFF1 and activation of NF-κB during the multistep human carcinogenesis cascade. In the human stomach, TFF1 protein is expressed predominantly in the superficial foveolar epithelium of the gastric body and antrum (5, 31), and this expression is frequently lost in human gastric cancer (32, 33). qRT-PCR analysis of *TFF1* in 70 human gastric tumors revealed a significant overall reduction of *TFF1* expression in tumors as compared with 36 normal gastric epithelia samples ($P < 0.001$) (Supplemental Figure 8, A and B). IHC staining of p–NF-κB–p65 and TFF1 on human gastric tissue samples revealed strong immunostaining of TFF1 in normal gastric mucosa, whereas p–NF-κB–p65 staining was absent to weak (Figure 9, A and E). We also observed strong immunostaining of p–NF-κB–p65 and absence of TFF1 in intestinal metaplasia and dysplasia (Figure 9, B and F). Gastric adeno-

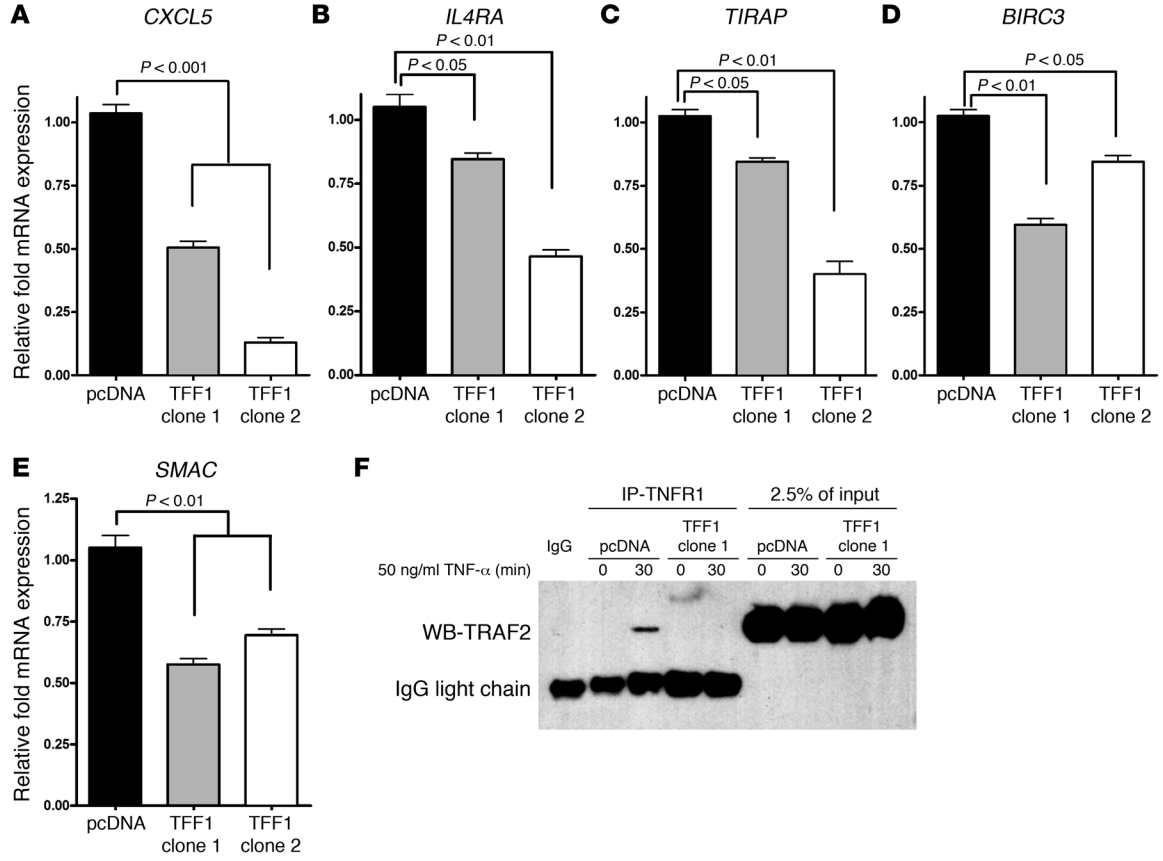

Figure 8

TFF1 suppresses TNF-α–induced upregulation of NF-κB target genes through TNFR1. (**A**–**E**) qRT-PCR showing a decrease in mRNA expression of pro-inflammatory genes (*CXCL5*, *IL4R*, *TIRAP*) and anti-apoptotic genes (*BIRC3*, *SMAC*) in AGS-TFF1 cells relative to AGS-pcDNA cells, following 8 hours of treatment with TNF-α. The bar graphs represent the mean ± SEM of 3 independent experiments. (**F**) Immunoprecipitation with TNFR1 in AGS-pcDNA and AGS-TFF1 clone 1. The cells were treated with TNF-α (50 ng/ml) for 30 minutes or left untreated (control). Immunoprecipitations were carried out with mouse TNFR1 antibody. The first lane exhibits AGS-pcDNA following immunoprecipitation with mouse IgG control antibody. All immunoprecipitations and their corresponding input samples were subjected to immunoblotting with rabbit polyclonal antibody against TRAF2. As shown in AGS-pcDNA cells, the TNFR1 immunoprecipitate demonstrated the presence of TRAF2, which was not detected in the AGS-TFF1 cells. The results represent 1 of at least 3 independent experiments.

carcinomas showed strong immunostaining of p–NF-κB–p65 and weak to absent immunostaining of TFF1 (Figure 9, C and G). To investigate the expression of these two proteins in the multistep progression cascade of gastric cancer, we developed a composite expression score (CES) as described in the Methods. Our results showed an inverse trend between TFF1 and p–NF-κB–p65 expression scores ($P = 0.09$), after adjusting for the effects of histology and interaction between NF-κB and histology. We also investigated the potential relationship between TFF1, NF-κB expression, and the gastric tumorigenesis cascade using this linear model, as defined above. The results demonstrated a strong, statistically significant inverse correlation ($P < 0.001$) between TFF1 expression and progression from normal mucosa toward cancer. In contrast, there was a statistically significant positive correlation ($P < 0.001$) between p–NF-κB–p65 and the progression from normal mucosa towards cancer (Figure 9, D and H).

Discussion

TFF1 is a secreted protein expressed predominantly by the gastric epithelia and upregulated in response to injury (2, 5). The frequent loss of *TFF1* expression in more than two-thirds of gastric carcinomas occurs through a combination of genetic and epigenetic mechanisms (7–9, 13). In this study, we have performed a systematic study to define the histological, molecular, and signaling components of the *Tff1*-knockout mouse model (17) in order to understand the development of gastric neoplasia. We showed inflammation and age-associated progressive histological events in *Tff1*-knockout mice in the pyloric antrum of gastric mucosa from gastritis toward HGD and malignant adenocarcinoma. As lesions became more severe, we observed the presence of acute inflammation that progressed to chronic inflammation as characterized by the presence of inflammatory cells in the submucosa and their infiltration in the glandular epithelia. The role of inflammation in carcinogenesis is supported by the observation of reduced risk of many cancers following the long-term use of NSAIDs (34). In this regard, the development of human gastric adenocarcinoma is strongly linked to age and chronic inflammation (35), which can be considered as an added source of cancer risk that is responsible for retention of inflammatory angiogenesis and immune suppression (36). Hence, this chronic inflammation initiates histopatho-

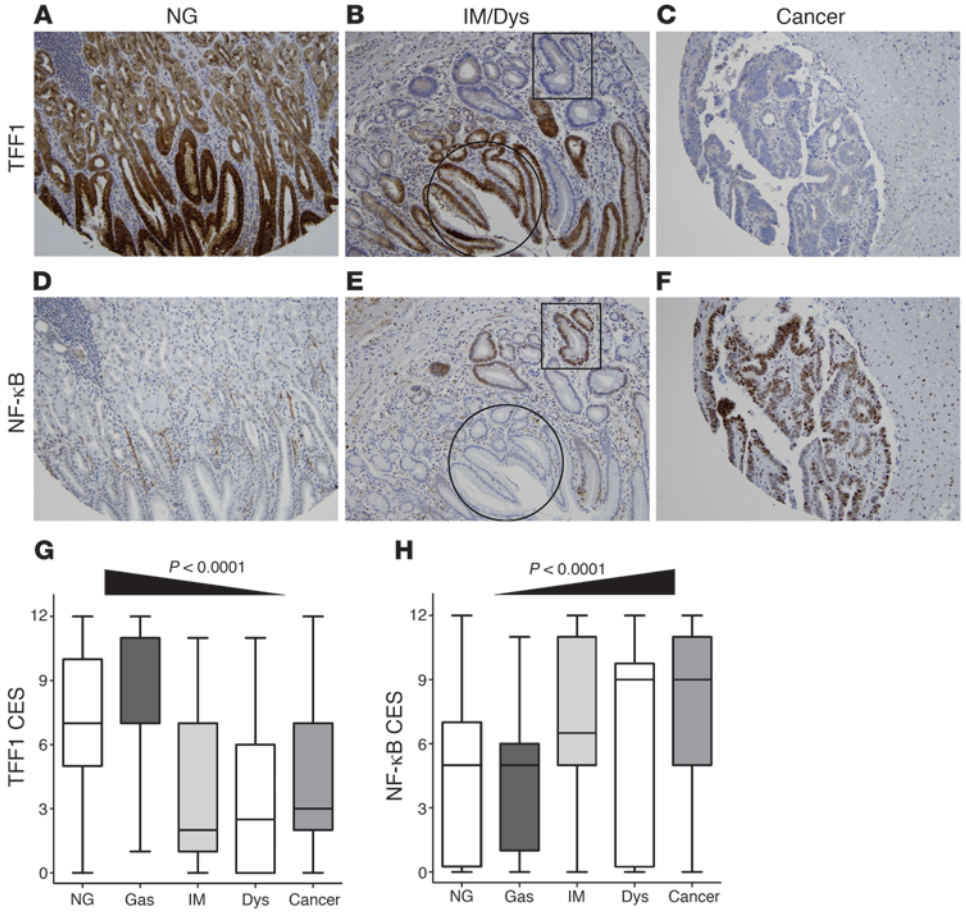

Figure 9
Immunohistochemistry for TFF1 and NF-κB in human samples. (**A**–**F**) Immunohistochemical staining for TFF1 and NF-κB in serial tissue sections from human gastric mucosa with normal histology (NG; **A** and **D**), intestinal metaplasia and dysplasia (IM/Dys; **B** and **E**), and adenocarcinoma (**C** and **F**). A progressive decrease of TFF1 expression was observed from normal mucosa to adenocarcinoma, along with a progressive increase in p–NF-κB–p65 expression. The circular and rectangular areas demonstrate an inverse relationship in the immunostaining of TFF1 and p–NF-κB–p65 in serial sections from the same tissue. Original magnification, ×20. (**G** and **H**) The graphs summarize the immunohistochemical staining results on gastric tissue microarrays.

logic progression from chronic gastritis to gastric atrophy, intestinal metaplasia, dysplasia, and finally gastric cancer (1, 35). Our data suggest that this cascade of events and increase of chronic inflammation in *Tff1*-knockout mice resulted from loss of *Tff1* gene in gastric tissue, and specifically in the antropyloric area. Long-term treatment with a broad spectrum of antibiotics did not reduce the chronic inflammation scores. In addition, administration of celecoxib and NSAIDs and Cox-2–selective inhibition in *Tff1*-knockout mice were sufficient to reduce dysplastic lesions by 50%. Indeed, this effect was associated with the reduction of the proinflammatory genes *Cxcl1* and *Cxcl5*. Therefore, this could explain the link between inflammation and tumorigenesis in our *Tff1*-knockout mouse model.

In an attempt to define the molecular underpinnings of the loss of TFF1 in gastric tumorigenesis, we initially performed a comprehensive gene expression analysis. The molecular signature in the *Tff1*-knockout mouse model pointed to deregulation of several hundred genes. Of note, 76 genes were inflammation related, and we validated several key pro-inflammatory genes such as *Tnfa*, *Il1b*, and *Cxcl1*, *-2*, and *-5*. This is consistent with the published data, indicating that the transcription of pro-inflammatory cytokines stimulates the proliferation of tumor and stromal cells to further fuel tumor growth (23). Several clinical studies have suggested that polymorphisms in pro-inflammatory cytokine genes such as *IL1B* and *TNFA* are associated with gastric cancer (37, 38). In fact, a recent study demonstrated that gastric-specific overexpression of human *IL1B* in transgenic mice is sufficient for stepwise progression of gastric dysplasia and cancer (39). Therefore, the development and progression of lesions in the *Tff1*-knockout mouse model mimics, to a large extent, human disease.

Network analysis of gene expression data is a powerful tool to identify critical pathways that are likely involved with the molecular signature. This analysis suggested that the NF-κB pathway might be a central transcriptional hub involved in the regulation of a large number of inflammation-related and pro-survival genes in gastric tissues of the *Tff1*-knockout mouse model. NF-κB transcription factors are rapidly activated in response to various stimuli, including cytokines, infectious agents, and radiation-induced DNA double-strand breaks. Elevated NF-κB activity in premalignant epithelial cells suppresses apoptosis, thereby promoting their survival and subsequent capacity to form tumors (38). The results from the ex vivo immunofluorescence of pyloro-antral epithelial cells demonstrated significant nuclear localization of NF-κB, indicative of its transcriptional activity. In fact, several validated genes in our study are known targets of NF-κB transcription factors, such as *TNFA*, *IL1B*, *IL4R*, and *CXCL1*, *-2*, and *-5*. To further validate the role of TFF1 in regulating NF-κB, we utilized the NF-κB reporter that contains binding sites of NF-κB as a measure of activation of NF-κB transcription activity using AGS cells as a human gastric cancer cell model. In all assays, TFF1 suppressed TNF-α–mediated activation of NF-κB reporter. In the absence of cellular stimuli, NF-κB transcription factors are bound to inhibitory IκB proteins and are thereby sequestered in the cytoplasm. Two protein kinases with a high degree of sequence similarity, IKKα and IKKβ, mediate

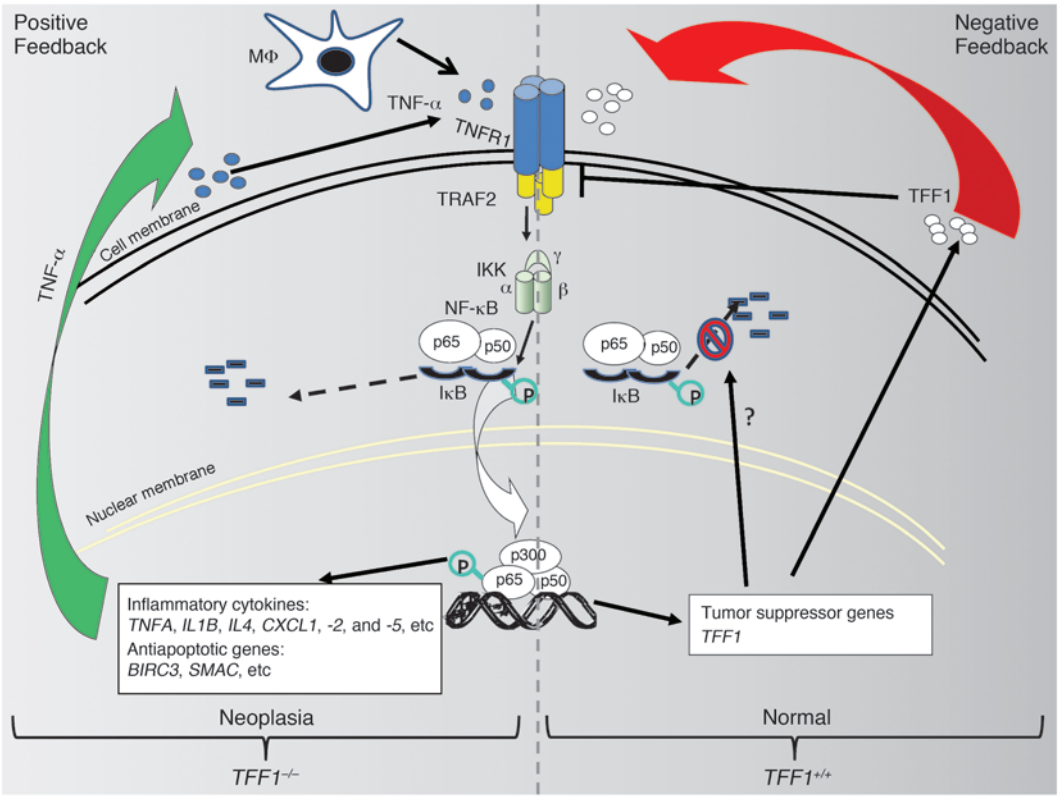

Figure 10
A diagram depicting the role of TFF1 in regulating inflammation in gastric epithelial cells. The development of gastric cancer is associated with an inflammatory phenotype that could mediate the release of TNF-α. The TNF-α–induced activation of NF-κB leads to upregulation of several chemokines and pro-survival genes that mediate the inflammatory phenotype. One of the transcription targets of NF-κB is TFF1, which acts as a negative feedback loop that attenuates TNF-α–mediated activation of NF-κB. With the silencing of *TFF1* gene in gastric cancers (LOH and methylation); the NF-κB could become hyperactive due to loss of the TFF1 inhibitory functions.

phosphorylation of IκB proteins and represent a convergence point for most signal transduction pathways, leading to NF-κB activation (21, 29). In response to activating stimuli, IκB proteins are phosphorylated, leading to their subsequent recognition by ubiquitinating enzymes and degradation. The proteasomal degradation of IκB proteins liberates IκB-bound NF-κB, which translocates to the nucleus to drive expression of target genes (29). These kinases are essential for rapid NF-κB activation by pro-inflammatory signaling cascades, such as those triggered by TNF-α (29). We have provided the first evidence that loss of TFF1 leads to activation of the NF-κB transcription factors regulated via the IKK complex. We have also shown that reconstitution of TFF1 in AGS cells, as well as the addition of conditioned media from these cells to primary gastric epithelial cells, interfere with the activation of NF-κB, and the replacement of TFF1-conditioned media with conditioned media from AGS-pcDNA rescues this activation. These results suggest the cell-autonomous function of antropyloric epithelial cells that can be independent of stromal cells.

TNFR1 is the primary receptor triggering TNF-α–mediated induction of NF-κB transcription factors (29, 40). TNF-α activates IKK signaling cascade through TNFR1 and TRADD/RIP/TRAF2 complex, leading to activation of NF-κB transcription factors (29, 41). We investigated whether TFF1 blocks the transduction of the activating signal via interference with the formation of TRADD/RIP/TRAF2 complex by examining binding of TRAF2 and TNFR1 after reconstitution of TFF1 expression. Indeed, expression of TFF1 abrogated the binding of TNFR1 to TRAF2 following conditions of TNF stimulation, thus interfering with TNF-α–mediated activation of NF-κB transcription factors. Of note, a recent study has shown an NF-κB binding site at –231 bp of the *TFF1* gene promoter that plays a central role in induction of TFF1 transcription in response to TNF-α (42). In view of this study and our findings, the TFF1/NF-κB regulation is a complex process, and our results suggest the presence in epithelial cells of a negative feedback regulatory loop that enables control of the NF-κB–mediated inflammatory response to minimize epithelial cell damage (Figure 10). Our immunohistochemical analysis of human tissues demonstrated a modest increase in the TFF1 level in chronic gastritis lesions as compared with normal gastric epithelia. This increase was followed by a significant reduction in TFF1 levels in the subsequent progression steps toward gastric cancer. During the progression to gastric cancer, *TFF1* is silenced by genetic and epigenetic mechanisms in the majority of gastric cancers (7–9). We have demonstrated suppression of several known pro-inflammatory and anti-apoptotic NF-κB target genes following the restoration of TFF1 expression in the in vitro AGS cell model. Taken together, our results suggest that the loss of TFF1 disrupts the negative feedback loop, leading to an unchecked upregulation of

NF-κB that mediates the expression of pro-inflammatory and anti-apoptotic genes; both effects favor the expansion of epithelial cells, facilitating neoplastic transformation and cancer progression.

The major challenge in many studies is to validate the findings made in mice in human cancer patients. Our analysis of a large number of tissue samples that represent the histological development and progression steps of gastric cancer demonstrated a significant downregulation of *TFF1* and activation of NF-κB as lesions progressed toward gastric adenocarcinoma. These data not only validate the mouse data, but also reveal the possibility of developing novel and improved therapeutic and preventive strategies that could reduce the burden of gastric cancer.

In summary, the *Tff1*-knockout mouse model recapitulates the classical chronological cascade of human multistage gastric carcinogenesis due to TFF1 deficiency. Our in vivo and in vitro data strengthen the link between the loss of TFF1 and the development of gastric cancer. We provide what is, to our knowledge, the first evidence that loss of TFF1 leads to activation of the NF-κB transcription factors regulated via the IKK complex, thus elucidating the critical role of TFF1 loss in coupling inflammation and gastric tumorigenesis. This observation provides a general understanding of the role of inflammation in gastric carcinogenesis and demonstrates that TFF1 plays an important role in shaping the NF-κB–mediated inflammatory response in the multistep gastric tumorigenesis cascade.

Methods

Animals: histologic evaluation and immunohistochemical assessment. C57BL/6J/129/Svj mixed genetic background *Tff1*-knockout and normal *Tff1* wild-type mice (17) were used in this study. Tissue samples were collected from 126 *Tff1*-knockout and 44 *Tff1* wild-type mice. All animals were approved by the Institutional Animal Care and Use Committee at Vanderbilt University and were maintained under barrier conditions in a pathogen-free state. Following euthanasia, animals were dissected through midline incision of the abdomen. Stomachs were removed, cut along the lesser curvature, washed with PBS, and opened to lie flat. The stomachs were examined visually for abnormalities and for size and number of individual gastric tumors and photographed. The stomach was cut into symmetrical halves. One half was submerged in 10% buffered formalin solution, embedded in paraffin, and processed for standard H&E staining for histopathology evaluation. Classification and grading of the gastric tissues were performed by our pathologists. Proliferating cells were detected with a mouse monoclonal antibody directed against the Ki-67 antigen (Sigma-Aldrich). The remaining half of the stomach was snap-frozen and stored at –80°C for further use.

Gene expression microarray analysis. Four *Tff1*-knockout and 3 *Tff1* wild-type mice were sacrificed at the age of 12 months. The stomachs were excised and opened along the lesser curvature and processed for frozen sections for laser capture microdissection. All the *Tff1*-knockout gastric tissues had HGD, whereas all wild-type mice had histologically normal stomachs. Gastric epithelial cells (10,000–16,000 cells per sample) from the antrum region were microdissected using a PixCell IIe laser capture microdissection microscope (Arcturus/Molecular Devices) using a 30-micron spot size and 60- to 80-mW laser pulse. Total RNA was isolated using an RNeasy Mini kit (Qiagen). Quality of RNA was evaluated using a 2100 Bioanalyzer (Agilent Technologies), and RNA samples used for microarrays had an RNA integrity number of 7 or greater. RNA samples with these quality standards were reverse transcribed and amplified using a WT-Ovation Pico RNA amplification kit and labeled with FL-Ovation cDNA Biotin module v2 (both from NuGen). Amplified products were hybridized to Affymetrix Mouse 430 2.0 microarrays (Affymetrix), following the manufacturers' recommendations, by the Vanderbilt Functional Genomics Shared Resource. Gene expression in microdissected gastric epithelial cells was compared between *Tff1*-knockout mice ($n = 4$) and *Tff1* wild-type mice ($n = 3$). The raw gene expression data (.cel files) were preprocessed and normalized by using the robust multi-array average (RMA) expression measure, with RMA function in Bioconductor package affy (http://www.bioconductor.org/packages/release/bioc/html/affy.html) (43). The expression values were in $\log_2$ format after RMA (43). Bioconductor package limma was used for array data analysis (http://www.bioconductor.org/packages/release/bioc/html/limma.html) (44). A linear model was fitted to the expression data for each probe. Moderated *t* statistics were computed by empirical Bayes shrinkage of the standard errors toward a common value. The *P* values corresponded to the moderated *t* statistics. We used both *P* values as well as fold change to determine candidate probe list by requiring at least 2.8-fold change ($\log_2[\text{fold}] \geq 1.5$) and $P \leq 0.05$, using R software version 2.10.0 (45). Last, the data sets of normalized expression values plus their associated gene identifiers were uploaded into IPA software (Ingenuity Systems) to generate biological networks. This was performed by mapping values and gene identifiers (GenBank accession) to their corresponding gene objects in the Ingenuity Knowledge Base (Ingenuity Systems) developed from published sources (Ingenuity Systems).

Primary gastric epithelial cell extraction and short-term culture. For preparation of short-term cultures of primary gastric epithelial cells from the *Tff1*-knockout and wild-type mice, stomachs were removed from 8-week-old mice and opened as described above. After washing with HBSS, the gastric antrum was cut and incubated in 10 ml of 1 mM dithiothreitol for 15 minutes at 37°C with shaking, washed in HBSS 3 times at 37°C, and incubated in 0.5 mg/ml collagenase for 30 minutes at 37°C. After the first collagenase digestion, tissues were washed again with HBSS 3 times and incubated for an additional 30 minutes in collagenase (0.37 mg/ml) at 37°C. Tissues were triturated using a wide-mouthed pipette, and larger fragments of tissue were allowed to settle under gravity for 45 seconds. The supernatant containing isolated gastric cells was removed and transferred to a clean 50-ml conical tube and left on ice to sediment for 45 minutes. The supernatant was then carefully removed and discarded, and isolated cell colonies were plated in chamber slides. Colonies of gastric epithelial cells were cultured in F-12 (Ham's medium) supplemented with 10% FBS and 1% of antibiotic-antimycotic solution (Invitrogen Life Technologies). The cells were incubated in a humidified incubator at 37°C under an atmosphere of 5% CO_2. Cell colonies were cultured for up to 72 hours, and the medium was changed every 24 hours.

Reconstitution of TFF1 expression in cell lines. AGS cells were obtained from ATCC and were cultured in Ham's F-12 supplemented with 10% FBS (Invitrogen Life Technologies) at 37°C in an atmosphere containing 5% CO_2. In order to reconstitute the expression of TFF1 in AGS cells, we established AGS cell lines stably expressing human TFF1. The human *TFF1* coding sequence was amplified using PCR and cloned in-frame into pcDNA3.1 mammalian expression vector (Invitrogen) following standard protocols. AGS cells were transfected with pcDNA3.1-TFF1 or empty vector (control) using Fugene-6 (Roche Applied Science) following the manufacturer's protocols. Stable transfectants were selected using 0.5 mg/ml G418 (Invitrogen). After 3 weeks of selection, several cell colonies were isolated using cloning rings and then transferred to fresh plates. Single-colony cultures were identified and analyzed by qRT-PCR. AGS-TFF1 clones that had high expression levels of *TFF1* were used in the study.

Immunofluorescence assay. Primary gastric epithelial cells prepared as described above, and AGS gastric cancer cells stably expressing TFF1 or empty vector (control) were plated in 8-well chambers. Cells were washed with PBS and fixed with fresh 4% paraformaldehyde solution for 15 minutes at room temperature. Cells were then washed twice with PBS, followed by incubation in 10% normal goat serum blocking solution (Zymed Labora-

tories) for 20 minutes at room temperature in a humidified chamber. Cells were incubated in the specific primary antibodies against NF-κB–p65 (Gene Script) diluted in PBS (1:400) for 2 hours at room temperature in a humidified chamber. Cells were washed 3 times in PBS and incubated in fluorescein isothiocyanate–tagged secondary antibody (1:1,000; Jackson Immunoresearch) for 45 minutes at room temperature in a humidified chamber. The cells were then washed in PBS, mounted with Vectashield/DAPI (Vector Laboratories), and visualized using an Olympus BX51 fluorescence microscope (Olympus Co.). At least 200 cells were counted from each experiment. Total cell number was measured with automatic particle counting in ImageJ software (http://www.uhnresearch.ca/facilities/wcif/imagej/), after setting an automatic threshold range. The image was transformed into a binary image, and the total number of cells in each field was counted using watershed separation. The percentage of NF-κB–p65–positive cells was calculated as the number of cells showing nuclear green staining divided by the total cell number showing DAPI nuclear blue staining × 100.

qRT-PCR. Total RNA was isolated using the RNeasy Mini kit (Qiagen), and single-stranded cDNA was subsequently synthesized using the Advantage RT-for-PCR Kit (Clontech Laboratories Inc). Genes specific for mouse and human primers were designed using the online software Primer 3 (http://frodo.wi.mit.edu/primer3/). The forward and reverse primers were designed to span 2 different exons for each gene (mouse: *Tff1*, *Tnfa*, *Il1b*, *Il1a*, *Cxcl1*, *Cxcl2*, *Cxcl5*, *Il4ra*, *Vtcn1*, and *Apoa1*; human: *TFF1*, *CXCL5*, *IL4RA*, *TIRAP*, *BIRC3*, *SMAC*, *TNFR1*, and *TNFR2*). All primers were purchased from Integrated DNA Technologies (Supplemental Table 2). The qRT-PCR was performed using an iCycler (Bio-Rad), with the threshold cycle number determined by use of iCycler software version 3.0. Reactions were performed in triplicate, and the threshold cycle numbers were averaged. The results of the genes were normalized to housekeeping genes, *HPRT* for human and *b-actin* for mouse, as described previously (46). Expression ratios were calculated according to the formula $2^{(Rt-Et)}/2^{(Rn-En)}$ (46), where *Rt* is the threshold cycle number for the reference gene observed in the test samples, *Et* is the threshold cycle number for the experimental gene observed in the test samples, *Rn* is the threshold cycle number for the reference gene observed in the reference samples, and *En* is the threshold cycle for the experimental gene observed in the reference samples. *Rn* and *En* values were calculated as an average of all reference samples.

Luciferase reporter assay. To monitor the activity of the NF-κB signal transduction pathway, we used the pNF-κB–Luc reporter vector, which contains multiple copies of the NF-κB consensus sequence (Clontech). After endogenous NF-κB proteins bind to the κ enhancer element, transcription is induced and the reporter gene is activated. Cells (1×10^4) were seeded in 96-well plates. The next day, cells were transiently transfected with 60 ng of the NF-κB–Luc reporter and 6 ng of a ubiquitin promoter *Renilla* luciferase control plasmid using Fugene6 according to the manufacturer's instructions (Roche Applied Science). Twenty-four hours after transfection, cells were treated with 50 ng/ml of TNF-α (Pepro Tech) and/or 400 ng/ml of recombinant protein TFF1 (Novus Biologicals) for 24 hours and harvested. Luciferase activity was measured using the Dual-Luciferase Reporter Assay kit (Promega) according to the manufacturer's instructions. Firefly luciferase activities were normalized to *Renilla* luciferase levels. Results are the average of 3 independent experiments and are expressed as mean values (± SEM).

Western blotting. Cell lysates were prepared in RIPA buffer containing Halt Protease Inhibitor Cocktail and Halt Phosphatase Inhibitor Cocktail (Pierce Biotechnology Inc.), and were centrifuged at 4,390 *g* for 10 minutes at 4°C. Protein concentration was measured using a Bio-Rad Protein Assay (Bio-Rad Laboratories). Proteins (10–15 μg) from each sample were subjected to SDS/PAGE and transferred onto nitrocellulose membranes. Target proteins were detected by using specific antibodies against IKKβ, p-IKKα/β (Ser176/180), IκB, p-IκB (Ser32), and β-actin (Cell Signaling Technology).

For assay of nuclear translocation of NF-κB, nuclear and cytoplasmic protein fractions were isolated from stably transfected cell lines, pcDNA and TFF1, using NE-PER Nuclear and Cytoplasmic Extraction Reagents (Pierce Biotechnology Inc.) following the manufacturer's instructions. Equal amounts of nuclear and cytoplasmic proteins (10 μg) were loaded onto 10% SDS-PAGE, separated by electrophoresis, and transferred to nitrocellulose membrane. The membranes were incubated with NF-κB–p65 and p–NF-κB–p65 (Ser536) antibodies (Cell Signaling Technology Inc.). The cytoplasmic and nuclear protein fractions were normalized to β-actin and lamin B (Santa Cruz Biotechnology Inc.), respectively

Immunoprecipitation. Cells were washed with cold PBS; 1 ml of cell lysis buffer from an MCL1-1KT Mammalian Cell Lysis Kit (Sigma-Aldrich) was added to the cells, which were rocked for 15 minutes at room temperature. Lysates were scraped and centrifuged for 10 minutes at 12,000 *g* at 4°C. Immunoprecipitation was performed using Dynabead Protein G (Dynal; Invitrogen Life Sciences) according to the manufacturer's instructions. TNFR1 antibody (Santa Cruz Biotechnology Inc.) was cross-linked to Dynabead Protein G. The cell lysate was added to the cross-linked beads and incubated for 1 hour with rocking at room temperature. The Dynabeads were then pelleted using a magnet and washed 3 times with washing buffer. Captured proteins were eluted from the beads by adding 40 μl of 2× protein-loading buffer to each sample and boiling for 5 minutes. Samples were resolved by SDS/PAGE and subjected to Western blotting. The membrane was incubated with TRAF2 antibody (Cell Signaling) overnight and followed by incubation with Mouse Anti-Rabbit IgG (Light-Chain Specific) monoclonal secondary antibody (Cell Signaling).

Human tissue microarrays and immunohistochemistry. Tissue microarrays containing cores from paraffin-embedded stomach tissue samples (39 normal mucosa, 43 gastritis, 88 intestinal metaplasia, 27 dysplasia, and 102 adenocarcinoma) were available for immunohistochemical analysis. All tissue samples were collected, coded, and de-identified using protocols approved by the Vanderbilt University Institutional Review Board. Tissues were stained with H&E, and representative regions were selected for inclusion in a tissue array. Tissue cores with a diameter of 0.6 mm were retrieved from selected regions of the donor blocks and punched to the recipient block using a manual tissue array instrument (Beecher Instruments). Samples were punched in triplicate, and control samples from normal mucosa specimens were punched in each sample row. Sections (5-μm) were transferred to polylysine-coated slides (SuperFrostPlus; Menzel-Glaser) and incubated at 37°C for 2 hours. The resulting tumor tissue array was used for immunohistochemical analysis. The adenocarcinomas collected ranged from well-differentiated (WD) to poorly differentiated (PD), stages I to IV, with a mix of intestinal and diffuse-type tumors. An avidin-biotin immunoperoxidase assay was performed after pretreatment for 20 minutes in a microwave oven with citrate buffer. Rabbit p–NF-κB–p65 (Ser536) antibody (1:200 dilution; Cell Signaling) and mouse Estrogen Inducible Protein pS2 (Tff1) antibody (1:200 dilution; Abcam) were applied at room temperature. In order to obtain a continuous score that takes into account the IHC signal intensity and the frequency of positive cells, we generated a CES with a full range from 0 to 12 (Supplemental Table 3). The CES was calculated using the formula CES = 4 (intensity – 1) + frequency (47).

Statistics. Using GraphPad Prism software, a 2-tailed Student's *t* test was used to compare the statistical difference between 2 groups, and a 1-way ANOVA Newman-Keuls Multiple Comparisons Test was used to compare the differences between 3 groups or more. The correlation between 2 parameters, age and chronic inflammation scores, was determined by Spearman correlation. The differences were considered statistically significant when the *P* value was ≤ 0.05.

To determine whether TFF1 and NF-κB have an inverse relationship, the following linear model was applied: TFF1 ~*NF-κB + grp + MFkB × grp*, where TFF1 is the TFF1 CES, *MFkB* is the NF-κB CES, and *grp* is the histology index for both TFF1 and NF-κB. The histology index is defined as a 5-level ordinary variable: 1 (normal), 2 (gastritis), 3 (intestinal metaplasia), 4 (dysplasia), and 5 (cancer).

Acknowledgments

This study was supported by the NIH grants R01CA93999, R01CA106176, R01DK58587, R01CA77955, and R01CA116087 and by the Prevent Cancer Foundation. The use of molecular and biostatistical cores was supported by the Digestive Disease Research Center (DDRC) DKP30DK058404 and Vanderbilt-Ingram Cancer Center (VICC) P30CA068485. The contents of this work are solely the responsibility of the authors and do not necessarily represent the official views of the National Cancer Institute or Vanderbilt University.

Received for publication December 4, 2010, and accepted in revised form January 26, 2011.

Address correspondence to: Wael El-Rifai, Vanderbilt University Medical Center, 1255 Light Hall, 2215 Garland Avenue, Nashville, Tennessee 37232, USA. Phone: 615.322.7934; Fax: 615.322.7852; E-mail: wael.el-rifai@vanderbilt.edu.

1. Correa P. A human model of gastric carcinogenesis. *Cancer Res*. 1988;48(13):3554–3560.
2. Thim L, May FE. Structure of mammalian trefoil factors and functional insights. *Cell Mol Life Sci*. 2005;62(24):2956–2973.
3. Ribieras S, Tomasetto C, Rio MC. The pS2/TFF1 trefoil factor, from basic research to clinical applications. *Biochim Biophys Acta*. 1998;1378(1):F61–F77.
4. Corte MD, et al. Cytosolic levels of TFF1/pS2 in breast cancer: Their relationship with clinical-pathological parameters and their prognostic significance. *Breast Cancer Res Treat*. 2006;96(1):63–72.
5. Rio MC, et al. Breast cancer-associated pS2 protein: synthesis and secretion by normal stomach mucosa. *Science*. 1988;241(4866):705–708.
6. Taupin D, Pedersen J, Familari M, Cook G, Yeomans N, Giraud AS. Augmented intestinal trefoil factor (TFF3) and loss of pS2 (TFF1) expression precedes metaplastic differentiation of gastric epithelium. *Lab Invest*. 2001;81(3):397–408.
7. Carvalho R, et al. Loss of heterozygosity and promoter methylation, but not mutation, may underlie loss of TFF1 in gastric carcinoma. *Lab Invest*. 2002; 82(10):1319–1326.
8. Katoh M. Trefoil factors and human gastric cancer (review). *Int J Mol Med*. 2003;12(1):3–9.
9. McChesney PA, et al. Cofactor of BRCA1: a novel transcription factor regulator in upper gastrointestinal adenocarcinomas. *Cancer Res*. 2006; 66(3):1346–1353.
10. Park WS, et al. Mapping of a new target region of allelic loss at 21q22 in primary gastric cancers. *Cancer Lett*. 2000;159(1):15–21.
11. Ribieras S, Lefebvre O, Tomasetto C, Rio MC. Mouse Trefoil factor genes: genomic organization, sequences and methylation analyses. *Gene*. 2001; 266(1–2):67–75.
12. Fujimoto J, Yasui W, Tahara H, Tahara E, Kudo Y, Yokozaki H. DNA hypermethylation at the pS2 promoter region is associated with early stage of stomach carcinogenesis. *Cancer Lett*. 2000;149(1–2):125–134.
13. Tomita H, et al. Inhibition of gastric carcinogenesis by the hormone, gastrin, is mediated by suppression of TFF1 epigenetic silencing [published online ahead of print November 25, 2010]. *Gastroenterology*. doi: 10.1053/j.gastro.2010.11.037.
14. Park WS, et al. Somatic mutations of the trefoil factor family 1 gene in gastric cancer. *Gastroenterology*. 2000;119(3):691–698.
15. Sankpal NV, Mayo MW, Powell SM. Transcriptional repression of TFF1 in gastric epithelial cells by CCAAT/enhancer binding protein-beta. *Biochim Biophys Acta*. 2005;1728(1–2):1–10.
16. Calnan DP, Westley BR, May FE, Floyd DN, Marchbank T, Playford RJ. The trefoil peptide TFF1 inhibits the growth of the human gastric adenocarcinoma cell line AGS. *J Pathol*. 1999;188(3):312–317.
17. Lefebvre O, et al. Gastric mucosa abnormalities and tumorigenesis in mice lacking the pS2 trefoil protein. *Science*. 1996;274(5285):259–262.
18. Barnes PJ, Karin M. Nuclear factor-kappaB: a pivotal transcription factor in chronic inflammatory diseases. *N Engl J Med*. 1997;336(15):1066–1071.
19. Karin M, Lawrence T, Nizet V. Innate immunity gone awry: linking microbial infections to chronic inflammation and cancer. *Cell*. 2006;124(4):823–835.
20. Karin M. Nuclear factor-kappaB in cancer development and progression. *Nature*. 2006; 441(7092):431–436.
21. Karin M. The IkappaB kinase - a bridge between inflammation and cancer. *Cell Res*. 2008; 18(3):334–342.
22. Greten FR, et al. IKKbeta links inflammation and tumorigenesis in a mouse model of colitis-associated cancer. *Cell*. 2004;118(3):285–296.
23. Karin M, Greten FR. NF-kappaB: linking inflammation and immunity to cancer development and progression. *Nat Rev Immunol*. 2005;5(10):749–759.
24. Luo JL, Kamata H, Karin M. IKK/NF-kappaB signaling: balancing life and death--a new approach to cancer therapy. *J Clin Invest*. 2005;115(10):2625–2632.
25. Pikarsky E, et al. NF-kappaB functions as a tumour promoter in inflammation-associated cancer. *Nature*. 2004;431(7007):461–466.
26. Yan F, Polk DB. Disruption of NF-kappaB signalling by ancient microbial molecules: novel therapies of the future? *Gut*. 2010;59(4):421–426.
27. Baeuerle PA, Baltimore D. NF-kappa B: ten years after. *Cell*. 1996;87(1):13–20.
28. Li H, Lin X. Positive and negative signaling components involved in TNFalpha-induced NF-kappaB activation. *Cytokine*. 2008;41(1):1–8.
29. Häcker H, Karin M. Regulation and function of IKK and IKK-related kinases. *Sci STKE*. 2006; 2006(357):re13.
30. Shu HB, Takeuchi M, Goeddel DV. The tumor necrosis factor receptor 2 signal transducers TRAF2 and c-IAP1 are components of the tumor necrosis factor receptor 1 signaling complex. *Proc Natl Acad Sci U S A*. 1996;93(24):13973–13978.
31. Hanby AM, Poulsom R, Singh S, Elia G, Jeffery RE, Wright NA. Spasmolytic polypeptide is a major antral peptide: distribution of the trefoil peptides human spasmolytic polypeptide and pS2 in the stomach. *Gastroenterology*. 1993;105(4):1110–1116.
32. Henry JA, Bennett MK, Piggott NH, Levett DL, May FE, Westley BR. Expression of the pNR-2/pS2 protein in diverse human epithelial tumours. *Br J Cancer*. 1991;64(4):677–682.
33. Westley BR, Griffin SM, May FE. Interaction between TFF1, a gastric tumor suppressor trefoil protein, and TFIZ1, a brichos domain-containing protein with homology to SP-C. *Biochemistry*. 2005; 44(22):7967–7975.
34. Baron JA, Sandler RS. Nonsteroidal anti-inflammatory drugs and cancer prevention. *Annu Rev Med*. 2000;51:511–523.
35. Fox JG, Wang TC. Inflammation, atrophy, and gastric cancer. *J Clin Invest*. 2007;117(1):60–69.
36. Schwartsburd PM. Age-promoted creation of a pro-cancer microenvironment by inflammation: pathogenesis of dyscoordinated feedback control. *Mech Ageing Dev*. 2004;125(9):581–590.
37. Murphy G, et al. Association of gastric disease with polymorphisms in the inflammatory-related genes IL-1B, IL-1RN, IL-10, TNF and TLR4. *Eur J Gastroenterol Hepatol*. 2009;21(6):630–635.
38. Machado JC, et al. A proinflammatory genetic profile increases the risk for chronic atrophic gastritis and gastric carcinoma. *Gastroenterology*. 2003; 125(2):364–371.
39. Tu S, et al. Overexpression of interleukin-1beta induces gastric inflammation and cancer and mobilizes myeloid-derived suppressor cells in mice. *Cancer Cell*. 2008;14(5):408–419.
40. Mauro C, Zazzeroni F, Papa S, Bubici C, Franzoso G. The NF-kappaB transcription factor pathway as a therapeutic target in cancer: methods for detection of NF-kappaB activity. *Methods Mol Biol*. 2009; 512:169–207.
41. Katoh M. AP1- and NF-kappaB-binding sites conserved among mammalian WNT10B orthologs elucidate the TNFalpha-WNT10B signaling loop implicated in carcinogenesis and adipogenesis. *Int J Mol Med*. 2007;19(4):699–703.
42. Koike T, et al. Up-regulation of TFF1 (pS2) expression by TNF-alpha in gastric epithelial cells. *J Gastroenterol Hepatol*. 2007;22(6):936–942.
43. Irizarry RA, et al. Exploration, normalization, and summaries of high density oligonucleotide array probe level data. *Biostatistics*. 2003;4(2):249–264.
44. Smyth GK. Linear models and empirical bayes methods for assessing differential expression in microarray experiments. *Stat Appl Genet Mol Biol*. 2004;3:Article3.
45. R Development Core Team. *R: A Language And Environment For Statistical Computing*. Vol. 1. Vienna, Austria: R Foundation for Statistical Computing; 2009.
46. El-Rifai W, et al. Gastric cancers overexpress S100A calcium-binding proteins. *Cancer Res*. 2002; 62(23):6823–6826.
47. Mukherjee K, et al. Dopamine and cAMP regulated phosphoprotein MW 32 kDa is overexpressed in early stages of gastric tumorigenesis. *Surgery*. 2010; 148(2):354–363.